

Adversarial Examples for k -Nearest Neighbor Classifiers Based on Higher-Order Voronoi Diagrams

Chawin Sitawarin
UC Berkeley

Evgenios M. Kornaropoulos
UC Berkeley

Dawn Song
UC Berkeley

David Wagner
UC Berkeley

Abstract

Adversarial examples are a widely studied phenomenon in machine learning models. While most of the attention has been focused on neural networks, other practical models also suffer from this issue. In this work, we propose an algorithm for evaluating the adversarial robustness of k -nearest neighbor classification, i.e., finding a minimum-norm adversarial example. Diverging from previous proposals, we take a geometric approach by performing a search that expands outwards from a given input point. On a high level, the search radius expands to the nearby Voronoi cells until we find a cell that classifies differently from the input point. To scale the algorithm to a large k , we introduce approximation steps that find perturbation with smaller norm, compared to the baselines, in a variety of datasets. Furthermore, we analyze the structural properties of a dataset where our approach outperforms the competition.

1 Introduction

It is well-known that machine learning models can easily be misled by maliciously crafted inputs, called adversarial examples, generated by adding a tiny perturbation to test samples (Biggio et al., 2013; Szegedy et al., 2013; Goodfellow et al., 2015). Adversarial examples are often studied in the context of neural networks, leaving the problem largely unexplored for other classifiers. The k -nearest neighbor, or simply k -NN, classifier is a simple yet widely used model in various applications such as recommendation systems. This non-parametric classifier does not require a training phase and has a well-understood and elegant geometric foundation (Okabe et al., 1992). Recent works (Papernot and McDaniel, 2018; Dubey et al., 2019; Sitawarin and Wagner, 2019b) combine k -NN with neural networks to enhance the robustness and the interpretability

of the overall model. Despite the importance of k -NN, there are only a handful of works that study its robustness (Wang et al., 2018; Yang et al., 2020; Wang et al., 2019; Sitawarin and Wagner, 2019a, 2020).

The typical first step towards evaluating the robustness of a classifier is the task of generating an adversarial example that is close to a given test point, under some definition of closeness. For the case of k -NN where $k > 1$, this problem is challenging because it involves computing on high-dimensional polytopes that satisfy a set of geometric properties, the so-called Voronoi cells.

In this work, we propose the GeoAdEx algorithm for finding adversarial examples for k -NN classifiers. GeoAdEx is the first algorithm that exploits the underlying geometry of the k -NN classifier. Specifically, our approach performs a principled search on the underlying high-order Voronoi diagram by expanding the search radius around the test point until it finds an adversarial classification. The geometric foundation of GeoAdEx allows us to locate nearby adversarial cells that the other attacks typically miss. GeoAdEx follows the footsteps of the recent work by Jordan et al. (2019) who exploited the geometry of neural networks for verifying the outputs. Our algorithmic approach stands in sharp contrast to previous attacks for k -NN (Yang et al., 2020; Wang et al., 2019) which refine the exhaustive approach by heuristic-based filtering.

Furthermore, we introduce optimizations and approximations to the main algorithm and as a result the experiments show that GeoAdEx discovers the smallest adversarial distance compared to all baselines in the vast majority of our experiments for $k \in \{3, 5, 7\}$. GeoAdEx finds up to 20% smaller mean adversarial distance compared to the second best attack. We note that one inherent shortcoming of our geometric approach is the increased computation time, an aspect that can be further improved.

Finally, we present experiments that demonstrate that GeoAdEx performs significantly better when points from different classes are mixed together. On a high level, such a setup generates a more intricate spatial

tessellation with nearby cells that alternate classes. In this challenging case, GeoAdEx performs up to $5\times$ better than the baselines.

2 Background and Related Work

2.1 Background

Let $X = (x_1, \dots, x_n)$ be a set of points from \mathbb{R}^d , also called *generators*, and let $Y = (y_1, \dots, y_n)$ be the class of each point from the universe of possible classes $\{1, \dots, c\}$. Let $d(x, x')$ denote the L_2 norm for $x, x' \in \mathbb{R}^d$. Let $Z^{(k)}(X)$ be the set of all possible subsets consisting of k points from X , i.e., $Z^{(k)}(X) = \{L_1^{(k)}, \dots, L_i^{(k)}, \dots, L_l^{(k)}\}$, where $L_i^{(k)} = \{x_{i1}, \dots, x_{ik}\}$, $x_{ij} \in X$ and $l = \binom{n}{k}$. We define as *order- k Voronoi cell* associated with $L_i^{(k)}$ the set $V(L_i^{(k)})$ that includes the points of \mathbb{R}^d that are closer to $L_i^{(k)}$ than any other k points of X . More formally:

$$V(L_i^{(k)}) = \left\{ p \mid \max_x \{d(p, x) \mid x \in L_i^{(k)}\} \leq \min_{x'} \{d(p, x') \mid x' \in X \setminus L_i^{(k)}\} \right\}$$

With the term *Voronoi facet*, or simply *facet*, we refer to a boundary of an order- k Voronoi cell. We define as bisector $B\{x_a, x_b\}$ the set of points from \mathbb{R}^d that are equidistant from $x_a \in X$ and $x_b \in X$. There is a tight connection between bisectors and facets. Every Voronoi facet is part of a bisector, but not every bisector, $\binom{n}{2}$ in total, includes a Voronoi facet. We call the bisectors that do include a facet *active* bisectors and those that do not *inactive* bisectors. We also note that an order- k Voronoi cell has at most $k(n - k)$ facets. The collection of order- k Voronoi cells for all $L_i^{(k)}$ is called *order- k Voronoi diagram*. In this work, we assume the standard non-cocircularity assumption¹ to avoid degenerate cases. We only consider the Euclidean distance for the k -NN, i.e., $d(x_a, x_b) = \|x_a - x_b\|_2$.

Up to this point, we have not used the classes of the X . In this work, we focus on k -NN classifiers that classify based on the majority (class) vote of the k -nearest points. We define as *adversarial cell* with respect to (x, y) any order- k Voronoi cell that has different majority than label y . We denote with $A(x)$ the set of all adversarial cells with respect to (x, y) . With the term *adversarial facet* with respect to (x, y) we refer to a facet that belongs to a cell from $A(x)$.

¹In practice this can be achieved by adding a small random noise on each generator to break potential cocircularity between them.

2.2 Related Work

Adversarial Robustness of k -NN Classifiers.

Wang et al. (2018) study the robustness property of k -NN classifiers from a theoretical perspective. The authors show that a k -NN classifier can be as robust as the optimal Bayes classifier given a sufficiently large number of generators and k . Wang et al. (2018) and Yang et al. (2020) also propose potential methods for improving the robustness of k -NN by pruning away some of the “ambiguous” generators. Other works consider different alternatives for enhancing the robustness of neural networks by combining them with k -NN. (Papernot and McDaniel, 2018; Sitawarin and Wagner, 2019b; Dubey et al., 2019)

Attacks on k -NN Classifiers.

Sitawarin and Wagner (2019a, 2020) propose a method for finding minimum-norm adversarial examples on k -NN and deep k -NN classifiers (Papernot and McDaniel, 2018). Their method approximates a k -NN classifier with a soft differentiable function so adversarial examples can be found via a gradient-based optimization algorithm. While the approach is efficient and scalable to large k , it provides no guarantee for finding the nearest adversarial example and overlooks the geometry of k -NN.

Yang et al. (2020) and Wang et al. (2019) take a similar approach for finding the adversarial example closest to a given test x . Their method follows an exhaustive search by computing the distance between x and all the Voronoi cells that have a different class from x . Both Yang et al. and Wang et al. show that this can be done exactly when $k = 1$ but does not scale well for $k > 1$. Consequently, they introduce heuristics to improve the efficiency by choosing only a subset of the Voronoi cells. However, in the process, they lose the optimality guarantee on the resulted adversarial example. More importantly, the heuristics will miss an exponential number of cells as k increases.

Attacks Based on Geometry.

The problem of verifying or finding the nearest adversarial examples in neural networks is an active research direction where solutions still do not scale to a satisfactory degree (Huang et al., 2017; Katz et al., 2017; Tjeng et al., 2017; Wong and Kolter, 2018; Weng et al., 2018; Cohen et al., 2019; Jordan et al., 2019). Among these works, Jordan et al. (2019) proposed an alternative for a ReLU network, using a geometric approach. Specifically, the authors notice that piecewise linear networks partition the input space into numerous polytopes where points of the same polytope are classified with the same label. Armed with this observation, they propose an algorithm that iteratively searches through these polytopes that are further away from the test sample until they find a polytope with a different label.

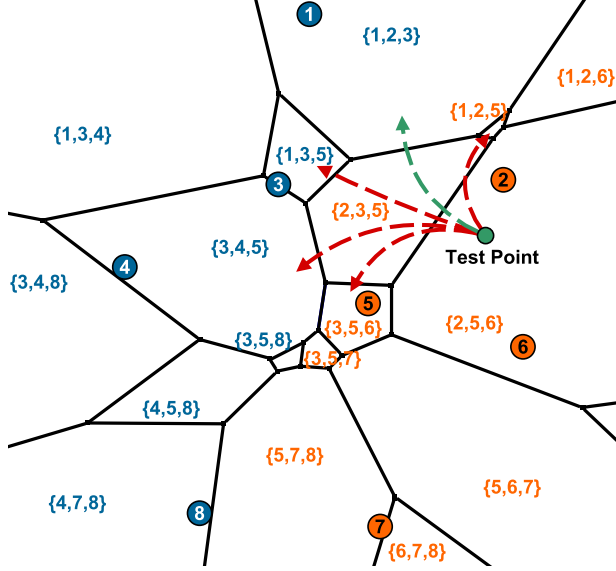


Figure 1: GeoAdEx on a Voronoi diagram for $k = 3$ in \mathbb{R}^2 with two classes. The color of each numbered generator point shows its class, and the color of the label of each cell indicates its classification outcome. The illustration presents the step where GeoAdEx has processed the facets of $V\{2, 5, 6\}$ and is transitioning to the next closest cell $V\{2, 3, 5\}$. The arrows indicate the facets that are inserted to the priority queue PQ . When GeoAdEx terminates, it outputs the closest adversarial facet; this transition is indicated with green.

3 The GeoAdEx Algorithm

Objective. The goal of the algorithm is to find the smallest perturbation δ^* that moves a test point (x, y) to an adversarial cell. This objective can be expressed as an optimization problem in the following form:

$$\begin{aligned} \delta^* = \arg \min_{\delta} \quad & \|\delta\|_2^2 \\ \text{s.t.} \quad & x + \delta \in A(x) \end{aligned} \quad (1)$$

We define as ϵ^* *optimal adversarial distance*, i.e., $\epsilon^* := \|\delta^*\|_2$. The norm of any other (non-optimal) perturbation δ that misclassifies (x, y) , i.e., $x + \delta \in A(x)$, is simply called *adversarial distance*.

A First Approach. The constraint of the above formulation implies that it is required for $x + \delta$ to be a member of an adversarial cell from $A(x)$. A simple approach to solve this minimization is to build a series of optimization problems, one for each of the cells in $A(x)$, and pick the solution with the minimum adversarial distance. Unfortunately, this would require solving $O(\binom{n}{k})$ quadratic programs each of which has $k(n - k)$ constraints. While this complexity may be manageable when $k = 1$ and n is small, it does not scale with k . On a high-level, Yang et al. and Wang et al. take this

approach and additionally develop heuristics in order to scale to cases with $k > 1$.

The GeoAdEx Approach. The core idea of GeoAdEx is to perform a principled *geometric exploration* around the test point x . GeoAdEx processes order- k Voronoi cells à la breadth-first search until it discovers an adversarial cell. Algorithm 1 provides a pseudocode of the main steps of GeoAdEx, and Figure 1 illustrates some steps of GeoAdEx on a 3-NN classifier with two classes.

We highlight that Algorithm 1 terminates when the *deleteMin* method of PQ outputs an adversarial facet. In the following subsections, we explain these steps in detail and describe performance speedups as well as approximation steps to scale the algorithm to $k > 1$.

Algorithm 1: GeoAdEx Algorithm

Data: Test point (x, y)

Result: Adversarial distance ϵ

- 1 Initialize the smallest adversarial distance ϵ found so far as $\epsilon \leftarrow \infty$;
 - 2 Initialize PQ by inserting the facets of the order- k Voronoi cell that x falls into. Mark this cell as *visited*;
 - 3 Call *deleteMin* from PQ until the returned facet is part of an unvisited order- k Voronoi cell. Initialize Ψ to this unvisited Voronoi cell;
 - 4 **while** Ψ is not an adversarial cell **do**
 - 5 Find the set of facets Φ that comprise unvisited cell Ψ (Section 3.2);
 - 6 Compute the distance between query point x and each of the facets in Φ (Section 3.3);
 - 7 If (i) a facet from Φ is an adversarial facet, and (ii) the distance to this adversarial facet implies a smaller norm than ϵ , then update ϵ ;
 - 8 Insert to PQ the facets in Φ with their distance if smaller than ϵ ;
 - 9 Call *deleteMin* from PQ until the returned facet is part of an unvisited order- k Voronoi cell. Update Ψ to the new unvisited Voronoi cell;
 - 10 **end**
 - 11 If an adversarial facet is removed from PQ via *deleteMin*, the algorithm return the optimal adversarial distance (see Lemma 1);
 - 12 **return** ϵ ;
-

3.1 Data Structures

We maintain a priority queue PQ as an auxiliary data structure that is defined for a given test point (x, y) . PQ tracks the progress made so far towards locating the optimal adversarial distance. Specifically, PQ performs the operations *insert* (resp. *deleteMin*) where the input (resp. output) is a facet of the order- k Voronoi diagram of X . Every facet in PQ is accompanied by the distance between the test point x and the facet. Priority is given to the facet with the *minimum* distance to x . We also need to mark which Voronoi cells are processed. For that, we use a dictionary that has an entry for every

order- k Voronoi cell that the algorithm has visited. We refer to Voronoi cells that are part of the dictionary as *visited* and those that are not as *unvisited*.

3.2 Find Neighbors of a Voronoi Cell

Line 3 & 9 of algorithm GeoAdEx discovers an *unvisited* order- k Voronoi cell Ψ . In Line 5 algorithm GeoAdEx needs to find the facets that comprise Ψ , which is equivalent to finding the order- k Voronoi cells that are *neighboring* with cell Ψ . We present three options for implementing the discovery of neighbors; the choosing among them depends on the application, the size of the dataset, and the value of k .

(A) Neighbors via Order- k Voronoi Diagram.

The exact computation of an order- k Voronoi diagram in high dimensions constitutes a computationally challenging task. The cost of this option amortizes when there is a large number of test points to be processed, and the dataset is fairly small in size and dimension. However, it is highly unlikely to scale when $k > 1$ which is the goal of our work.

(B) Neighbors via Enumerating Bisectors.

In this approach, one has to process a quadratic number of bisectors that are potentially *active* with respect to the Voronoi cell Ψ (see the definition from Section 2). Interestingly, we can filter out this set by only considering the bisectors where exactly one of the bisector's generator also generates cell Ψ . Consequently, we can reduce the task of finding the facets of the current cell Ψ to testing the *activeness* of $k(n-k)$ bisectors. Jumping ahead, this step can be accomplished simultaneously with computing distance from x to each bisector so we defer its analysis for Section 3.3. For comparison, the complexity of this step is $O(\text{poly}(n, d, k))$ without any speedups, and in the worst case, which is extremely unlikely in practice, it can be called up to N times where N is the number of all cells (N is $O(\binom{n}{k})$).

(C) Neighbors via Order-1 Voronoi Diagram.

This approach is the middle ground between the first two. That is, it still tests whether a bisector is active, much like (B), but it uses the Voronoi diagram, much like (A), to reduce the number of bisectors to test. Given a Voronoi cell with k generators, e.g., $V(\{x_1, \dots, x_{k-1}, x_k\})$, we know that its neighboring cells must have a set of generators that differs by exactly one point, e.g., $V(\{x_1, \dots, x_{k-1}, x_l\})$. We draw a connection between the Voronoi diagrams of order 1 and k and show that the new point x_l must be *neighboring with at least one of the order-1 cells* $V(\{x_1\}), V(\{x_2\}), \dots, V(\{x_k\})$. We formalize this in Theorem 1, and its proof can be found in Appendix D.

Theorem 1. *Let $S = \{x_1, \dots, x_{k-1}\} \subset X$ be a set of $k-1$ generators. Let $x_k, x_l \in X$ be two generators such*

that $x_k, x_l \notin S$. If $V(S \cup \{x_k\})$ and $V(S \cup \{x_l\})$ are two neighboring order- k Voronoi cells, then the order-1 Voronoi cell $V(\{x_l\})$ is neighboring with at least one of the $V(\{x_1\}), \dots, V(\{x_{k-1}\}), V(\{x_k\})$.

With this insight, we can *narrow down significantly* the number of bisectors considered in approach (B). More formally, let $nb(x')$ denote the set of generators of order-1 Voronoi cells that neighbor with $V\{x'\}$. Let Ψ be the Voronoi cell $V(\{x_1, \dots, x_k\})$. By Theorem 1, it is enough to consider the bisectors between $z \in \{x_1, \dots, x_k\}$ and $z' \in \left(\bigcup_{i=1}^k nb(x_i)\right) - \{x_1, \dots, x_k\}$. Hence, the total number of bisectors we need to test is at most $k \cdot |\bigcup_{i=1}^k nb(x_i)|$. Assuming that $\ell := \max_i |nb(x_i)|$, the number of bisectors cannot exceed $k^2 \ell$. Hence, approach (C) is much faster than approach (B) when $k^2 \ell \ll n$. In this work, we use approach (B) for the $k = 1$ case. However, in order to scale to large datasets and $k > 1$, we propose some approximations steps that are rooted on approach (C) later in Section 3.5.2.

3.3 Computing Distance & Testing Activeness

Now we describe Line 6 of Algorithm 1, i.e. how to compute the distance between a point x and a facet. Then, expanding on this process, we detail how to test the activeness of bisectors.

Distance computation. A Voronoi cell is a polytope that can also be described as an intersection of half-spaces: $\{z \mid Az \leq b\}$. A bisector can be described as a hyperplane: $\{z \mid \langle z, \hat{a} \rangle = \hat{b}\}$. The corresponding facet needs to both be part of the polytope *and* satisfy the equation of the hyperplane. Thus, the shortest distance from x to a facet is given by the square root of the optimum of the following quadratic program:

$$\begin{aligned} \min_z \quad & \|z - x\|_2^2 \\ \text{s.t.} \quad & Az \leq b \text{ and } \langle z, \hat{a} \rangle = \hat{b} \end{aligned} \tag{2}$$

This problem can be solved by any standard commercial solver, but in Section 3.5.1, we describe a much faster method also used by Wang et al.

Testing Bisector Activeness. Assuming that $\{z \mid Az \leq b\} \neq \emptyset$, the bisector $\langle z, \hat{a} \rangle = \hat{b}$ is active *if and only if* Eqn. (2) is feasible since their intersection has to be non-empty. In case this problem is infeasible, the bisector is inactive. From duality theory, we know that Eqn. (2), i.e. the primal, is feasible if and only if the dual objective is unbounded since the dual problem is always feasible in this case. Checking the unboundedness can be accomplished as we are solving Eqn. (2) in its dual form so we can combine the steps of “distance computation” and “testing activeness” into a single

function that either returns the distance or indicates that the bisector is inactive.

We do a total of three checks to determine the feasibility: (i) check if the dual objective converges fast. When unbounded, the dual objective diverges or keeps increasing with a constant rate or faster. Additionally, we test whether the KKT conditions hold at the end of the optimization. Namely, (ii) check if the primal residual is zero, and (iii) check if the complementary slackness is satisfied. When all three checks pass, we conclude that the bisector is active. Otherwise, it is considered inactive, and there is no need to finish the distance computation or insert it to PQ .

3.4 Optimality of GeoAdEx

Here, we formally state two lemmas that together prove the optimality of the output of GeoAdEx. The next lemma is straightforward to show as it is a direct consequence of Lemma C.2 from Jordan et al. (2019). For completion, we prove it in Appendix D.

Lemma 1 (Correctness of GeoAdEx). *Provided no time limit, GeoAdEx terminates when it finds the optimal adversarial examples or equivalently, one of the solutions of Eqn. (1).*

The next lemma states that if GeoAdEx terminates early, i.e., in case we enforce a time limit for performance purposes (see Section 3.5.2), it can still guarantee that the algorithm provides a lower bound to ϵ^* . Specifically, the distance of x from the most recent facet deleted from PQ serves as a lower bound to ϵ^* .

Lemma 2 (Lower bound guarantee). *If GeoAdEx terminates early, the distance from test point x to the last deleted facet from PQ is a lower bound to the optimal adversarial distance ϵ^* .*

We note that if GeoAdEx terminates early, then ϵ serves as an upper bound of ϵ^* . None of the previous approaches on adversarial examples for k -NN provide both an upper and lower bound guarantee.

3.5 Towards Scaling GeoAdEx

For simplicity, in Algorithm 1 we present the main algorithmic steps that need to be performed to compute the optimal adversarial distance using the geometric structure of the problem. In this section we delve into details on how to accelerate the performance of GeoAdEx by *performance optimization* and *approximation* steps.

3.5.1 Optimizing Computation Time

We introduce four main performance optimizations that significantly speed up GeoAdEx.

(I) Pruning Distant Facets. Given *any* adversarial distance, e.g., the intermediate result ϵ from Algorithm 1, we know that any facet that is more than ϵ afar from x is not the facet associated with the optimal adversarial distance, i.e., ϵ acts as an upper bound that is refined during the execution. Hence, we can safely filter out these facets, and we note that it is unnecessary to compute their distance to x , test activeness, or insert them to PQ . This observation can be used in a few places as a filtering criterion to avoid unnecessary computation.

For example, before computing the distance between x and a facet, as proposed in Section 3.3, we can first use ϵ to filter unnecessary computation. Specifically, we can compute the orthogonal projection of x onto the bisector implied by the facet. If the distance to the bisector, which is a lower bound on the distance to the facet, is larger than ϵ , then this facet can be safely discarded.

Even if we proceed with the distance computation, we can still use ϵ to terminate the optimization in Eqn. (2) early. Specifically, if the dual objective of Eqn. (2) surpasses ϵ^2 , we can terminate the solver and discard this facet since, from strong duality, the dual objective is a lower bound of the primal objective, i.e. the (squared) distance between x and this facet. A benefit of our principled geometric approach is that we can apply geometric arguments to eliminate redundant computation on Voronoi cells that are far away.

(II) Rethinking the Initialization of ϵ . Recall that Line 1 of Algorithm 1 initializes ϵ to ∞ . Given the “upgraded role” of ϵ that we presented in (I), it is clear that a non-simplistic initialization would filter out more unnecessary computation early on and, thus, scale the overall performance. For our experiments we run Sitawarin et al. to initialize ϵ since it yields a reasonable ϵ and is significantly faster than Yang et al. and Wang et al.

(III) Exploiting the Sparsity of Solutions. Solving a typical quadratic program has a complexity of $O(\text{poly}(n, d, k))$, but fortunately, this problem can be solved very efficiently in its dual form. Wang et al. (2019) show that solving Eqn. (2) via greedy coordinate ascent (GCA) is much faster than using a standard off-the-shelf solver as it is able to exploit the sparsity in the solution. More details about this speedup can be found in Appendix E.

(IV) Setting a Time Limit. To ensure that GeoAdEx terminates in a reasonable time even when no adversarial facet has been deleted from PQ , we set a time limit as a termination criterion. In this case, lower and upper bounds of ϵ^* are returned instead.

3.5.2 Acceleration via Approximations

As mentioned in Section 3.2, approach (C) for finding the neighbors of an order- k Voronoi cell still requires the knowledge of the first-order cells. This can be obtained by either computing the entire order-1 Voronoi diagram or enumerating all possible facets of order-1 cells. Nonetheless, first-order cells in a high-dimension dataset still have a large number of neighbors, and building a Voronoi diagram may easily become a bottleneck in high-dimensions. In this case, approach (C) is no better than approach (B) of Section 3.2. To scale to large and high-dimension datasets, we introduce some approximations. Here, we propose the *approximate version* of GeoAdEx built upon the relationship between order-1 and order- k neighbors from Theorem 1.

Description. To circumvent the expensive (in high dimensions) computation of the order-1 neighbors, we approximate approach (C) of Section 3.2. Specifically, instead of operating on the neighbors of the order-1 cell $V\{x_i\}$, we operate on a subset of m points chosen from the entire set of X according to a fast heuristic. In other words, $nb(x_i)$ is (roughly) approximated by a new subset of fixed size m denoted as $\widetilde{nb}_m(x_i)$. For cell $V\{x_1, \dots, x_k\}$ and a given generator x_i of this cell, we select from X the m closest points to x_i that are not in $\{x_1, \dots, x_k\}$. Mathematically, we define $\widetilde{nb}_m(x_i)$ as:

$$\widetilde{nb}_m(x_i) = \{x_j \in X \mid d(x_i, x_j) \leq d(x_i, x_{\pi(m)})\} \setminus \{x_1, \dots, x_k\}$$

where $x_{\pi(m)}$ is the m -th nearest neighbor of x_i . With the above heuristic we guarantee that for each cell, we only have to compute the distance (and test activeness) for at most k^2m facets and, thus, sidestep the computation of the first order Voronoi diagram in high dimensions. Each subsequent optimization problem has at most k^2m constraints. Finding m nearest points to a single point x_i is a well studied problem and can be *approximately* solved very fast (Johnson et al., 2017; Aumüller et al., 2017; Andoni et al., 2018).

Limitations due to Approximation. Due to the above approximation, it is possible that some of the true order-1 neighbors are not included in $\bigcup_{i=1}^k \widetilde{nb}_m(x_i)$. Hence, some active facets and cells may be missed completely². This leads to two limitations. The first is that we can no longer guarantee the optimality of GeoAdEx through Lemmas 1 and 2. In other words, we cannot conclude whether the adversarial distance

²Depending on the dataset and m , the chance of this happening may not be high for two reasons: (i) For a large k , $\bigcup_{i=1}^k \widetilde{nb}_m(x_i)$ becomes a large set and is likely to cover most, if not entire, $\bigcup_{i=1}^k nb(x_i)$. (ii) Even if we miss some cells or facets as neighbors of a particular order- k cell, they may still be picked up by the other cells.

returned by the approximate version of GeoAdEx is the optimal adversarial distance (or its lower bound).

The second limitation is that the approximation may have a domino effect on the correctness of the distance computation. Recall that in the exact version of GeoAdEx, we have shown that it is possible to replace the bisectors in the constraint of the optimization problem in Eqn. (2) with bisectors between $\{x_1, \dots, x_k\}$ and $\bigcup_{i=1}^k nb(x_i)$. But with the approximation, the new feasible set in Eqn. (2) becomes a *superset* of the one in the exact version. Consequently, the steps in Section 3.3 may falsely label an inactive bisector as active or return smaller distance than the true value.

Addressing Limitations. It seems that the first limitation cannot be addressed in a practical way. In fact, it is an inherent limitation of deploying heuristics to boost performance; a similar issue appears in Sitawarin et al. as well as the approximate version of Yang et al. and Wang et al. However, the second limitation can be addressed, and we do so by using the full set of bisectors when computing the distance and testing the activeness of adversarial facets, an approach that incurs a small computational cost. We do not need to do the same for non-adversarial cells since their distance and activeness do not affect the correctness of GeoAdEx.

4 Experiments

Datasets. The attacks are evaluated on seven datasets most of which were used in the experiments by Yang et al. Namely, we evaluate GeoAdEx in that following datasets: Australian, Covtype, Diabetes, Fourclass, and fmnist06 (a two-class subset of Fashion-MNIST). Additionally, we also evaluate on datasets Gaussian and Letters which have more classes and data points.

Hyperparameters. We evaluate all the baselines using their publicly available code and default hyperparameters. For fairness, we fine-tuned the hyperparameters for each baseline but did not observe any significant difference in their performance, see Appendix B.3. For GeoAdEx, we choose to compute distance to cell and set m to 40 and applied a time limit to 100 seconds per test point. All the experiments are run on a server with 128 CPU cores. For more details on the datasets and the experiments, we refer the reader to Appendix A.

4.1 Main Findings

Table 1 compares the proposed GeoAdEx attack against the three baselines with respect to the mean perturbation norm. Interestingly, GeoAdEx *outperforms the other baselines* in five of the seven datasets on all values of $k = 3, 5, 7$. In the other two datasets, the results are comparable. GeoAdEx performs notably well on

Table 1: Mean norm of the adversarial perturbations on 100 random test points across datasets (lower is better). The numbers in parentheses is the ratio of the mean perturbation norm found by GeoAdEx over that of the best baseline. The smallest mean perturbation norm among the attacks for each dataset and each k is bolded.

k	Attacks	Australian	Covtype	Diabetes	Fourclass	Gaussian	Letters	fmnist06
3	Sitawarin et al.	.516	.182	.119	.128	.056	.127	.217
	Yang et al.	.443	.287	.115	.127	.115	.131	.178
	Wang et al.	.455	.184	.118	.125	.083	.128	.183
	GeoAdEx	.445 (1.00)	.157 (0.86)	.098 (0.85)	.124 (0.99)	.043 (0.77)	.112 (0.88)	.204 (1.14)
5	Sitawarin et al.	.534	.224	.143	.128	.061	.132	.209
	Yang et al.	.524	.350	.184	.130	.178	.142	.226
	Wang et al.	.488	.237	.138	.128	.121	.135	.204
	GeoAdEx	.513 (1.05)	.197 (0.87)	.125 (0.90)	.126 (0.98)	.044 (0.72)	.124 (0.93)	.201 (0.98)
7	Sitawarin et al.	.548	.274	.163	.127	.063	.129	.217
	Yang et al.	.583	.397	.210	.136	.226	.156	.240
	Wang et al.	.525	.294	.157	.130	.150	.141	.221
	GeoAdEx	.539 (1.02)	.253 (0.92)	.147 (0.93)	.126 (0.99)	.050 (0.79)	.126 (0.97)	.210 (0.96)

datasets Gaussian and Covtype with approximately 10% – 20% smaller perturbation norm than the second best attack. Since the results of the exact attacks for $k = 1$ are not the main focus of this work, they appear in Appendix B.1.

We report that while our attack finds an adversarial distance that is closer to the optimal compared to the baselines, its main limitation is its runtime. In some cases, the runtime of GeoAdEx can be an order of magnitude larger than the second best attack.

It is also important to note that each of the proposed attacks (including GeoAdEx) performs better when the underlying data present certain structural properties. As a result, there is no single attack, so far, that performs universally better across all datasets. In Section 4.2, we explore the property of datasets that make our attack superior.

4.2 Advantages of a Geometric Search

Intuitively, GeoAdEx is based on a search that expands outwards from the original test point. As a result, it performs significantly better than the baselines when there exists an adversarial cell in relatively close proximity to the given test point. In other words, GeoAdEx performs really well on datasets when the class-conditioned distributions are closer or present significant “overlap.” In this case, GeoAdEx is less likely to miss small adversarial cells that are close to the test point as confirmed by the main experiment. We verify this hypothesis in the following experiment where we control the closeness of classes and study the performance of GeoAdEx compared to the baselines.

Experiments with Class Closeness. Given a dataset with c class-conditioned data distributions D_1, \dots, D_c , we can compute the minimum KL-

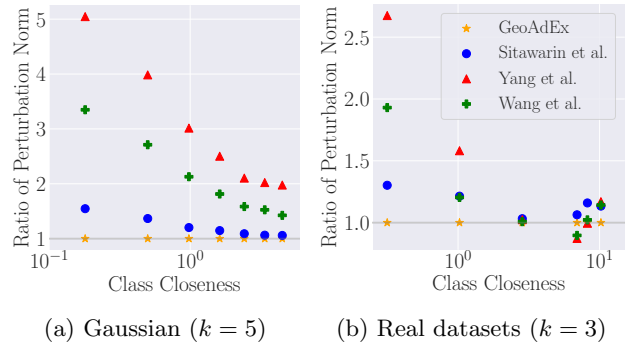


Figure 2: Mean perturbation norm found by the attacks as a function of the class closeness (lower is better).

divergence between a fixed distribution D_i and each of the other distributions D_j : $\text{KLD}(D_i||D_j)$. Now we define as *class closeness* the average of the above set of minima, i.e., $\frac{1}{c} \sum_{i=1}^c \min_j \text{KLD}(D_i||D_j)$. The smaller the class closeness, the closer their distributions are and, consequently the larger the degree of “mixing” between Voronoi cells of different classes. For each dataset, associated with a different value of class closeness, we record the ratio of the mean perturbation norm of each baseline over that of GeoAdEx.

First, we confirm this hypothesis on synthetic datasets where each of the two classes is generated by a Gaussian distributions, i.e., D_1, D_2 , in \mathbb{R}^{20} . Note that for Gaussian, KL-divergence can be analytically computed as the closed form exists. In this case, Figure 2a shows that GeoAdEx *significantly outperforms* all the baselines by a larger margin when the class closeness is small. That is, for the more challenging to classify datasets, which are the most interesting in practice, GeoAdEx outperforms the competition.

Furthermore, we revisit the real datasets from Table 1

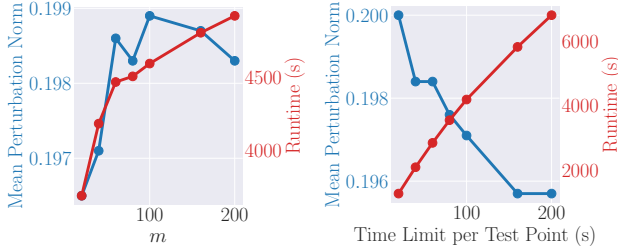


Figure 3: On Covtype ($k = 5$), we plot the mean perturbation norm and the total runtime of GeoAdEx against (left) m and (right) the time limit.

and re-interpret the results under the lens of their class closeness. Due to the fact that the true data distributions of these datasets are unknown, we *approximate* their KL-divergence via the data samples using the estimator in Equation (5) from Wang et al. (2009). Indeed, Figure 2b shows that the datasets from Table 1 for which GeoAdEx clearly outperforms the baselines, are the datasets with the smallest class closeness, that is Diabetes and Gaussian.

4.3 Ablation Study

In the following, we provide detailed results on GeoAdEx with respect to the choices of hyperparameters. According to Figure 3, by increasing m (the number of points chosen to approximate the first-order neighbors, see Section 3.5.2) and/or increasing the time limit beyond the reported values, we do not significantly affect the mean perturbation norm. A larger m increases the total runtime as GeoAdEx has to compute distance to more facets. In practice, a smaller m is preferable since it allows more cells to be explored even if this means that the approximation is coarser. Of course, if m is not large enough then the algorithm may miss numerous cells which, in turn, affects the performance. As expected, raising the time limit increases the total runtime and also finds adversarial examples with a smaller perturbation norm.

Next, we highlight the importance of the optimization steps (I) and (II) presented in Section 3.5.1. Specifically, we apply GeoAdEx on datasets Covtype and Diabetes for $k = 3$ where ϵ is naively initialized to ∞ , as opposed to the initialization from Section 3.5.1 (II). We observed that the total runtime increases by 62%, 15%, and 16%, for Covtype, Diabetes, and Letters, respectively.

5 Discussion & Open Problems

GeoAdEx has been shown to be successful in discovering adversarial examples for k -NN classifiers with $k \geq 1$. Compared to the baselines, GeoAdEx find adversarial examples with a considerably smaller perturbation

norm on average on most of the datasets.

The main limitation of GeoAdEx is its runtime. The approach by Sitawarin et al. is always the fastest, generally followed by Wang et al., Yang et al., and then GeoAdEx. With our choice of hyperparameters, GeoAdEx can be roughly an order of magnitude slower than Yang et al. and Wang et al. and two orders of magnitude slower than Sitawarin et al. In the interest of space, the runtime information is provided in Appendix B.2.

Scaling to a large k is a known challenge when attacking k -NN since the number of Voronoi cells increases exponentially in k . While Yang et al. and Wang et al. typically require less runtime than GeoAdEx, their results cannot be improved any further with more computation. Substantially increasing the runtime for Sitawarin et al. lowers the mean perturbation norm slightly, but it cannot beat GeoAdEx (see Appendix B.3).

We note that compared to the geometric approach by Jordan et al. (2019), our experiments were run on a significantly larger scale. Specifically, Jordan et al. (2019) was tested on neural networks with only up to 70 ReLUs which are much smaller than typical networks used in practice. GeoAdEx was tested on datasets with over ten thousand generator points and k up to 7, which results in a substantially larger number of polytopes to search through.

GeoAdEx has shown convincing results with our new geometric take on the problem, but there is room for improvements in terms of efficiency. Additional speedups can be introduced such as parallelization, GPU utilization, and a faster optimization technique. We believe that the approximation heuristic for determining the order-1 neighbors can also be improved. Furthermore, it is possible that the geometric properties of a high-order Voronoi diagram may be better exploited to save unnecessary computation on non-adversarial cells. For instance, multiple neighboring non-adversarial cells may be combined and approximated as a single large cell if we can guarantee that there is no adversarial cell inside this new polytope. This would remove a large number of distance computations surrounding the given test point, which is the main bottleneck of GeoAdEx. Additionally, GeoAdEx can also be directly extended to other space-partitioning classifiers such as decision trees and random forests.

6 Conclusion

We propose GeoAdEx, an algorithm based on geometric insights for finding adversarial examples on k -NN classifiers. Our experiments suggest that while using a higher computational cost, GeoAdEx significantly

outperforms the baselines on most of the datasets.

Acknowledgement

The first author of this paper was supported by the Hewlett Foundation through the Center for Long-Term Cybersecurity (CLTC), by the Berkeley Deep Drive project, and by gifts from Google and Futurewei.

The second and third authors were supported by the Center for Long-Term Cybersecurity (CLTC), by the Berkeley Deep Drive project, and by the NSF grant TWC-1518899.

References

- A. Andoni, P. Indyk, and I. Razenshteyn. Approximate nearest neighbor search in high dimensions. *arXiv preprint arXiv:1806.09823*, 7, 2018.
- M. Aumüller, E. Bernhardsson, and A. Faithfull. Ann-benchmarks: A benchmarking tool for approximate nearest neighbor algorithms. In *International Conference on Similarity Search and Applications*, pages 34–49. Springer, 2017.
- B. Biggio, I. Corona, D. Maiorca, B. Nelson, N. Šrndić, P. Laskov, G. Giacinto, and F. Roli. Evasion attacks against machine learning at test time. In H. Blockeel, K. Kersting, S. Nijssen, and F. Železný, editors, *Machine Learning and Knowledge Discovery in Databases*, pages 387–402, Berlin, Heidelberg, 2013. Springer Berlin Heidelberg. ISBN 978-3-642-40994-3.
- S. Boyd and L. Vandenberghe. *Convex Optimization*. Cambridge University Press, USA, 2004. ISBN 0521833787.
- C.-C. Chang and C.-J. Lin. LIBSVM: A library for support vector machines. *ACM Transactions on Intelligent Systems and Technology*, 2:27:1–27:27, 2011. Software available at <http://www.csie.ntu.edu.tw/~cjlin/libsvm>.
- J. M. Cohen, E. Rosenfeld, and J. Z. Kolter. Certified adversarial robustness via randomized smoothing. *arXiv preprint arXiv:1902.02918*, 2019.
- A. Dubey, L. van der Maaten, Z. Yalniz, Y. Li, and D. K. Mahajan. Defense against adversarial images using web-scale nearest-neighbor search. *CoRR*, abs/1903.01612, 2019.
- I. J. Goodfellow, J. Shlens, and C. Szegedy. Explaining and harnessing adversarial examples. In *International Conference on Learning Representations*, 2015.
- X. Huang, M. Kwiatkowska, S. Wang, and M. Wu. Safety verification of deep neural networks. In R. Majumdar and V. Kunčák, editors, *Computer Aided Verification*, pages 3–29, Cham, 2017. Springer International Publishing.
- J. Johnson, M. Douze, and H. Jégou. Billion-scale similarity search with gpus. *arXiv preprint arXiv:1702.08734*, 2017.
- M. Jordan, J. Lewis, and A. G. Dimakis. Provable certificates for adversarial examples: Fitting a ball in the union of polytopes. In *Advances in Neural Information Processing Systems*, pages 14082–14092, 2019.
- G. Katz, C. W. Barrett, D. L. Dill, K. Julian, and M. J. Kochenderfer. Reluplex: An efficient SMT solver for verifying deep neural networks. *CoRR*, abs/1702.01135, 2017. URL <http://arxiv.org/abs/1702.01135>.
- A. Okabe, B. Boots, and K. Sugihara. *Spatial Tessellations: Concepts and Applications of Voronoi Diagrams*. John Wiley & Sons, Inc., USA, 1992. ISBN 0471934305.
- N. Papernot and P. D. McDaniel. Deep k-nearest neighbors: Towards confident, interpretable and robust deep learning. *CoRR*, abs/1803.04765, 2018. URL <http://arxiv.org/abs/1803.04765>.
- C. Sitawarin and D. Wagner. On the robustness of deep k-nearest neighbors. volume abs/1903.08333, 2019a. URL <http://arxiv.org/abs/1903.08333>.
- C. Sitawarin and D. Wagner. Defending against adversarial examples with k-nearest neighbor. *arXiv preprint arXiv:1906.09525*, 2019b.
- C. Sitawarin and D. Wagner. Minimum-norm adversarial examples on knn and knn-based models. *ArXiv*, abs/2003.06559, 2020.
- C. Szegedy, W. Zaremba, I. Sutskever, J. Bruna, D. Erhan, I. J. Goodfellow, and R. Fergus. Intriguing properties of neural networks. *CoRR*, abs/1312.6199, 2013. URL <http://arxiv.org/abs/1312.6199>.
- V. Tjeng, K. Xiao, and R. Tedrake. Evaluating robustness of neural networks with mixed integer programming. *arXiv preprint arXiv:1711.07356*, 2017.
- L. Wang, X. Liu, J. Yi, Z.-H. Zhou, and C.-J. Hsieh. Evaluating the robustness of nearest neighbor classifiers: A primal-dual perspective. *arXiv preprint arXiv:1906.03972*, 2019.
- Q. Wang, S. R. Kulkarni, and S. Verdu. Divergence estimation for multidimensional densities via k -nearest-neighbor distances. *IEEE Transactions on Information Theory*, 55(5):2392–2405, 2009.
- Y. Wang, S. Jha, and K. Chaudhuri. Analyzing the robustness of nearest neighbors to adversarial examples. In J. Dy and A. Krause, editors, *Proceedings of the 35th International Conference on Machine Learning*, volume 80 of *Proceedings of Machine Learning Research*, pages 5133–5142, Stockholmsmässan, Stock-

holm Sweden, 10–15 Jul 2018. PMLR. URL <http://proceedings.mlr.press/v80/wang18c.html>.

T.-W. Weng, H. Zhang, H. Chen, Z. Song, C.-J. Hsieh, D. Boning, I. S. Dhillon, and L. Daniel. Towards fast computation of certified robustness for relu networks. *arXiv preprint arXiv:1804.09699*, 2018.

E. Wong and Z. Kolter. Provable defenses against adversarial examples via the convex outer adversarial polytope. volume 80 of *Proceedings of Machine Learning Research*, pages 5286–5295, Stockholmsmässan, Stockholm Sweden, 10–15 Jul 2018. PMLR. URL <http://proceedings.mlr.press/v80/wong18a.html>.

Y.-Y. Yang, C. Rashtchian, Y. Wang, and K. Chaudhuri. Robustness for non-parametric classification: A generic attack and defense. In *International Conference on Artificial Intelligence and Statistics*, pages 941–951. PMLR, 2020.

Appendix

A Details of the Experiments

Details regarding the datasets used in the experiments are included in Table 2. It also includes the accuracy of k -NN classifiers at $k = 1, 3, 5, 7$. Australian, Covtype, Diabetes, Fourclass, and fmnist06 are taken directly from Yang et al.’s implementation. The dataset fmnist06 is a two-class subset of Fashion-MNIST with a dimension reduction to 25 via PCA. The Letters dataset, together with the others, is taken from LIBSVM (Chang and Lin, 2011)³. Gaussian is a dataset we create by sampling from two isotropic Gaussian distributions of 20 dimension and variance of 1. The distance between the means of the two distributions is 1 by default and is varied only in Section 4.2 to get different values of class closeness.

All of the attacks are run on an Ubuntu (16.04) cluster with 128 AMD EPYC 7551 CPU cores (2.5GHz each) and 252 GB of memory. No GPU is used in any of the experiments. Using GPU could further speed up the attacks, but the official implementation of the baselines is not compatible with GPUs so we stick to CPUs to present a fair comparison. Yang et al. uses explicit parallelization and Cython C-extensions, whereas the rest of the attacks use pure Python code without explicit parallelization. The code for the baselines are taken directly from their respective public repository.⁴ Yang et al. uses Gurobi as the solver.

Table 2: Details of the datasets used in the experiments.

Datasets	# points	# features	# classes	$k = 1$ acc	$k = 3$ acc	$k = 5$ acc	$k = 7$ acc
Australian	490	14	2	0.805	0.805	0.830	0.845
Covtype	2000	54	7	0.755	0.715	0.730	0.705
Diabetes	568	8	2	0.695	0.755	0.695	0.685
Fourclass	662	2	2	1.000	0.995	1.000	1.000
Gaussian	10000	20	2	0.550	0.660	0.640	0.635
Letters	15000	16	26	0.925	0.940	0.940	0.930
fmnist06	12000	25	2	0.800	0.795	0.810	0.810

B Additional Results

B.1 Exact Attacks for $k = 1$

For completeness, we also compare the exact version of the attacks on 1-NN where the results are presented in Table 3. Note that Sitawarin et al. is excluded since it does not have an exact version. Wang et al. is generally the fastest, and GeoAdEx is faster than Yang et al., which does not seem to scale well with the number of generators and dimension. This is a direct effect of the solvers of the quadratic programs. Greedy coordinate ascent, used by Wang et al. and our attack, is much more efficient than a general-purpose commercial solver.

B.2 Runtime Comparisons

Table 4 includes the runtime of all the attacks for $k = 3, 5, 7$. For GeoAdEx, a “completed attack” means that the main steps of GeoAdEx manages to find an adversarial example with the distance smaller than the initialized one (see Section 3.5.1) before the time limit is reached. Otherwise, it simply returns the adversarial distance found by the attack we use to compute the initial ϵ , i.e. an incomplete attack. We note that this does not mean that GeoAdEx fails to find any adversarial example.

As we have mentioned, GeoAdEx with $m = 40$ and the time limit of 100 seconds takes longer to run compared to the other attacks for most cases. Sitawarin et al. is the fastest, followed by Wang et al. and Yang et al.. For the other cases, Yang et al. has the longest runtime. The reported runtime of GeoAdEx also includes the time used to initialize the adversarial distance ϵ found by Sitawarin et al..

³<https://www.csie.ntu.edu.tw/~cjlin/libsvmtools/datasets/multiclass.html>

⁴Sitawarin et al.: <https://github.com/chawins/knn-defense>, Yang et al.: <https://github.com/yangarbiter/adversarial-nonparametrics>, Wang et al.: https://github.com/wangwllu/knn_robustness

Table 3: Runtime for the exact version of the attacks on all of the datasets with $k = 1$. The numbers in the parentheses indicate the number of completed attack (out of 100) of GeoAdEx.

Attacks	Australian	Covtype	Diabetes	Fourclass	Gaussian	Letters	fmnist06
Yang et al.	72	7186	66	59	9109	34997	18461
Wang et al.	2	10	2	25	159	78	333
GeoAdEx	17 (100)	38 (100)	15 (100)	39 (100)	476 (100)	7450 (98)	19307 (99)

Table 4: Runtime (in seconds) for each of the attacks on all of the datasets. The numbers in the parentheses indicate the number of “completed” attacks (out of 100) of GeoAdEx.

k	Attacks	Australian	Covtype	Diabetes	Fourclass	Gaussian	Letters	fmnist06
3	Sitawarin et al.	28	40	26	6	12	34	15
	Yang et al.	201	1008	222	108	700	2402	3266
	Wang et al.	1001	788	321	383	226	346	350
	GeoAdEx	6417 (67)	1300 (82)	4159 (75)	3218 (63)	2699 (68)	5024 (49)	6751 (43)
5	Sitawarin et al.	24	33	24	6	12	34	15
	Yang et al.	316	2792	353	152	10140	11224	8284
	Wang et al.	1197	940	442	394	355	394	434
	GeoAdEx	8480 (23)	4182 (73)	6210 (57)	6208 (37)	4357 (73)	8305 (42)	7949 (32)
7	Sitawarin et al.	25	35	6	6	14	47	18
	Yang et al.	41	10585	26	199	16235	36331	15228
	Wang et al.	1553	1171	674	448	465	401	498
	GeoAdEx	9253 (14)	6064 (57)	7334 (38)	7481 (38)	6004 (65)	8955 (22)	9029 (27)

Note that the approximate version of Yang et al. and Wang et al. also terminates early by setting the maximum number of adversarial cells to search through instead of a hard limit on the runtime. In the next section, we show that increasing this number for Yang et al. and Wang et al. increases runtime but does not improve their results.

B.3 Attack Hyperparameters

Generally, the reported results are not very sensitive to the hyperparameter choices (see Table 5). We could not improve results from Yang et al. and Wang et al. further with more computation even after increasing the number of cells searched by these attacks by two and four times ($\times 2$ and $\times 4$). While the runtime increases significantly, changes on the mean perturbation norm remain essentially unchanged. On the contrary, there is small room for improvement for Sitawarin et al. as we simultaneously increase the number of random restarts, the number of iterations, and the frequency of threshold adjustment.

C Class Closeness

Intuitively, the *class closeness* measures distance between one distribution to another that has a different class and is closest to it. We only consider the closest class because when generating an adversarial example, one only has to perturb the test point towards the nearest distribution with a different class and the other classes are almost irrelevant. More formally, we can write the class closeness as

$$\text{class closeness} := \frac{1}{c} \sum_{i=1}^c \min_{j \in \{1, \dots, c\}} \text{KLD}(D_i || D_j)$$

where c is the number of classes, and D_i is the distribution conditioned on class i .

We first experiment with the Gaussian dataset because its KL-divergence has a analytical form. Specifically, the KL-divergence between two multivariate Gaussian distributions in \mathbb{R}^d , $D_1 = \mathcal{N}(\mu_1, \Sigma_1)$ and $D_2 = \mathcal{N}(\mu_2, \Sigma_2)$, is given by

$$\text{KLD}(D_1 || D_2) = \frac{1}{2} \left[\log \frac{|\Sigma_2|}{|\Sigma_1|} - d + \text{tr}(\Sigma_2^{-1} \Sigma_1) + (\mu_2 - \mu_1)^\top \Sigma_2^{-1} (\mu_2 - \mu_1) \right]$$

Table 5: Mean perturbation norm and runtime of the three baseline attacks when their hyperparameters vary.

Attacks	Hyperparameters	Covtype		Diabetes		Letters	
		Norm	Time	Norm	Time	Norm	Time
Sitawarin et al.	$\times 1$.1820	40	.1199	26	.1271	34
	$\times 2$.1728	125	.1070	72	.1211	263
	$\times 4$.1639	864	.1011	466	.1187	2398
Yang et al.	$\times 1$.2874	1086	.1515	14	.1311	2402
	$\times 2$.2874	1984	.1515	23	.1311	4667
	$\times 4$.2874	3946	.1515	37	.1311	9162
Wang et al.	$\times 1$.1849	788	.1181	321	.1288	346
	$\times 2$.1849	2324	.1181	645	.1288	946
	$\times 4$.1849	7298	.1181	862	.1288	3278

In particular, we use isotropic Gaussian distributions so the means and the covariance matrices can be simplified even further.

$$\mu_1 = \begin{bmatrix} \alpha \\ 0 \\ \vdots \\ 0 \end{bmatrix}, \mu_2 = \begin{bmatrix} -\alpha \\ 0 \\ \vdots \\ 0 \end{bmatrix}, \Sigma_1 = \Sigma_2 = I_d$$

Note that we pick $d = 20$, and without loss of generality, we can simply assign different values of α and $-\alpha$ to the first coordinate of μ_1 and μ_2 to vary the distance between the two means. We pick α among $\{0.3, 0.5, 0.7, 0.9, 1.1, 1.3, 1.5\}$. This specific case yields a very simple form of KL-divergence:

$$\text{KLD}(D_1||D_2) = 2\alpha^2$$

For the second part, since the distributions of the other datasets are unknown, we use a non-parametric method from Wang et al. (2009) to approximate the KL-divergence. This method only requires samples from the distributions and is coincidentally based on k -NN. We pick $k = 5$ for this approximation method which has nothing to do with the value of k in k -NN classifiers we experiment with.

D Proofs

D.1 Theorem 1

Now we restate Theorem 1 and then the proof.

Theorem 1. *Let $S = \{x_1, \dots, x_{k-1}\} \subset X$ be a set of $k - 1$ generators. Let $x_k, x_l \in X$ be two generators such that $x_k, x_l \notin S$. If $V(S \cup \{x_k\})$ and $V(S \cup \{x_l\})$ are two neighboring order- k Voronoi cells, then the order-1 Voronoi cell $V(\{x_l\})$ is neighboring with at least one of the $V(\{x_1\}), \dots, V(\{x_{k-1}\}), V(\{x_k\})$.*

Proof. Let $V(x'|G)$ denote the order-1 Voronoi cell for x' on the set of generators G . From property OK1 in Section 3.2.1 of Okabe et al. (1992) we know that the order- k Voronoi cell $V(S \cup \{x_i\})$ can be expressed as:

$$V(S \cup \{x_i\}) = \left(\bigcap_{l=1}^{k-1} V(x_l | (X \setminus (S \cup \{x_i\})) \cup \{x_l\}) \right) \cap V(x_i | X \setminus S)$$

From the fact that $V(S \cup \{x_i\})$ is a order- k Voronoi cell, we know that $V(S \cup \{x_i\})$ is nonempty. Let us assume for the sake of contradiction that $V(\{x_i\})$ is not neighboring with any of the $V(\{x_1\}), \dots, V(\{x_{k-1}\})$. Then we know that:

$$V(\{x_i\}) = V(x_i | X \setminus S)$$

This is because the removal of S from the set of generators of the Voronoi diagram did not affect $V(\{x_i\})$ since $V(\{x_i\})$ is not neighboring with any of $V(\{x_1\}), \dots, V(\{x_{k-1}\})$. Additionally, the removal of x_i from the set of generators in the term $V(x_l | x_l \cup (X \setminus S \cup \{x_i\}))$ is not affecting the corresponding cell, again, because $V(\{x_i\})$ is not neighboring with $V(\{x_1\}), \dots, V(\{x_{k-1}\})$. This implies that:

$$V(x_l | (X \setminus (S \cup \{x_i\})) \cup \{x_l\}) = V(x_l | (X \setminus S) \cup \{x_l\})$$

Using the above observations we can rewrite the first relation as:

$$V(S \cup \{x_i\}) = \left(\bigcap_{l=1}^{k-1} V(x_l | (X \setminus S) \cup \{x_l\}) \right) \cap V(\{x_i\})$$

For the last part of the proof we will show that the above intersection is empty which contradicts the fact that $V(S \cup \{x_i\})$ is a nonempty Voronoi cell. Notice that the changes in the set of generators that take place in the term $V(x_l | (X \setminus S) \cup \{x_l\})$ for $l = [1, k-1]$ do not affect the Voronoi cell of x_i . This means that even after the changes in the set of generators, the cell of x_i is a superset of $V(\{x_i\})$, or to put it differently, the polytope $V(x_l | (X \setminus S) \cup \{x_l\})$ never enters the area of $V(\{x_i\})$. As a result, none of these terms intersects with $V(\{x_i\})$. But this contradicts the fact that $V(S \cup \{x_i\})$ is nonempty. \square

D.2 Lemma 1: Correctness of GeoAdEx

Lemma 1 (Correctness of GeoAdEx). *Provided no time limit, GeoAdEx terminates when it finds the optimal adversarial examples or equivalently, one of the solutions of Eqn. (1).*

Lemma 1 can be obtained directly from a similar theorem in Jordan et al. (2019). We first restate this theorem and the definition of *polyhedral complex*. Then, we provide a short proof.

Theorem 2 (Correctness of GeoCert). *(Restate from Theorem C.2 in Jordan et al. (2019)) For a fixed polyhedral complex \mathcal{P} , a fixed input point x_0 and a potential function ϕ that is ray-monotonic, GeoCert returns a boundary facet with minimal potential Φ .*

Definition 1 (Polyhedral Complex). *(Restate from Definition 2 in Jordan et al. (2019)) A nonconvex polytope, described as the union of elements of the set $\mathcal{P} = \mathcal{P}_1, \dots, \mathcal{P}_k$ forms a polyhedral complex if, for every $\mathcal{P}_i, \mathcal{P}_j \in \mathcal{P}$ with nonempty intersection, $\mathcal{P}_i \cap \mathcal{P}_j$ is a face of both \mathcal{P}_i and \mathcal{P}_j .*

Proof. In order to apply Theorem 2 to GeoAdEx, we need to show two things: (i) the test point lies in a polyhedral complex, and (ii) Euclidean distance is a ray-monotonic potential function.

First, it is trivial to see that the set of non-adversarial Voronoi cells connected to and including the cell the test input x falls into forms a polyhedral complex. Since Voronoi cells are polytopes and any pair of them intersect at most at the shared facet, any set of Voronoi cells forms a polyhedral complex. This (informally) proves part (i).

For part (ii), we refer the readers to Corollary C.3 of Jordan et al. (2019) which shows that Euclidean distance is a ray-monotonic potential function. With these two conditions in mind, GeoAdEx behaves in the same way as GeoCert algorithmically in their respective settings, and so Theorem 2 directly applies to GeoAdEx as well. \square

D.3 Lemma 2: Lower Bound of the Optimal Adversarial Distance

Lemma 2 (Lower bound guarantee). *If GeoAdEx terminates early, the distance from test point x to the last deleted facet from PQ is a lower bound to the optimal adversarial distance ϵ^* .*

Theorem 3. *(Restate from Lemma C.1 in Jordan et al. (2019)) For any polyhedral complex \mathcal{P} point x_0 , and ray-monotonic potential ϕ , let \mathcal{F}_i be the facet popped at the i -th iteration of GeoCert. Then for all $i < j$, $\Phi(\mathcal{F}_i) < \Phi(\mathcal{F}_j)$.*

Proof. From Lemma 1, the first adversarial facet deleted from PQ is the nearest one to x , and if that happens, GeoAdEx terminates. It is implied by Theorem 3 that the facets are always deleted from PQ in an ascending order of their distance to x . Combining these two facts, we can conclude that the distance of any facets deleted before the adversarial one is always smaller than ϵ^* . \square

E Distance Computation with Greedy Coordinate Ascent

We first restate the distance computation from Eqn. (2):

$$\begin{aligned} \min_z \quad & \|z - x\|_2^2 \\ \text{s.t.} \quad & Az \leq b \end{aligned}$$

Note that without loss of generality, the equality constraint $\langle z, \hat{a} \rangle = \hat{b}$ can be subsumed by the inequality. Now we provide the dual form of Eqn. (2):

$$\begin{aligned} \max_{\lambda} \quad & g(\lambda) := -\frac{1}{2} \lambda^\top A A^\top \lambda + \lambda^\top (Ax - b) \\ \text{s.t.} \quad & \lambda \geq 0 \end{aligned}$$

In the case that the primal and the dual problems are feasible, we know that strong duality holds because the objective is convex quadratic, and the constraints are affine (Boyd and Vandenberghe, 2004). Thus, by setting the derivative of the Lagrangian to zero, we have that $z^* = x + A^\top \lambda^*$.

According to the complementary slackness from the KKT conditions, we know that $\lambda_i^* \neq 0$ if and only if $\langle a_i, z^* \rangle = b_i$, which geometrically corresponds to z^* lying on the i -th bisector associated with a_i and b_i . Intuitively, it is unlikely that z^* lies on an intersection of many bisectors. Hence, there should be very few indices i such that $\lambda_i^* \neq 0$. This is the condition that makes solving the dual problem with greedy coordinate ascent very fast (Wang et al., 2019).

Greedy coordinate ascent (or descent) optimizes the variable only one coordinate per iteration, and there are multiple rules for choosing the coordinate at each iteration. Here, we follow Wang et al. (2019) and simply pick the i -th coordinate of λ such that its projected gradient is the largest. We describe greedy coordinate ascent in Algorithm 2. To avoid the full gradient computation at every iteration, we keep track and update it given that λ only changes by one coordinate.

Algorithm 2: Greedy Coordinate Ascent

Data: Test point (x, y) , Voronoi cell described by $Az \leq b$

Result: Projection of x onto the Voronoi cell

```

1 Initialize  $\lambda \leftarrow \mathbf{0}$ 
2 for  $t \in \{1, \dots, T\}$  do
3    $\nabla g(\lambda) \leftarrow -A A^\top \lambda + Ax - b$ 
4    $j \leftarrow \arg \max_i |(\max\{\lambda + \nabla g(\lambda), 0\} - \lambda)_i|$ 
5    $\lambda_j \leftarrow \max \left\{ \lambda_j + \frac{\nabla g(\lambda)_j}{\|a_j\|_2^2}, 0 \right\}$ 
6 end
7 return  $z = x + A^\top \lambda$ 

```
